Applied Catalysis B: Environmental 330 (2023) 122579

Contents lists available at ScienceDirect

Applied Catalysis B: Environmental

journal homepage: www.elsevier.com/locate/apcatb

A novel $SO_3\bullet^-$ mediated photoelectrocatalytic system based on MoS_2/Fe_2O_3 and CuNW@CF for the efficient treatment of sulfurous and nitrogenous oxides

Changhui Zhou [a], Jinhua Li [a,c,*], Yan Zhang [a], Jing Bai [a,c], Pengbo Wang [a], Bo Zhang [a], Lina Zha [a], Mingce Long [a], Baoxue Zhou [a,b,c,*]

[a] School of Environmental Science and Engineering, Key Laboratory of Thin Film and Microfabrication Technology (Ministry of Education), Shanghai Jiao Tong University, Shanghai 200240, PR China
[b] Shanghai Institute of Pollution Control and Ecological Security, Shanghai 200092, PR China
[c] Yunnan Key Laboratory of Pollution Process and Management of Plateau Lake-Watershed, Yunnan 650034, PR China

ARTICLE INFO

Keywords:
$SO_3\bullet^-$
Sulfurous and nitrogenous oxides
Photoelectrocatalytic
CuNW@CF
MoS_2/Fe_2O_3

ABSTRACT

Sulfurous and nitrogenous oxides, including NO_x and SO_2, and the generated substances NO_x^- and SO_3^{2-} widely exist in air and water as pollutants and thus are difficult to control in the environment. In this study, we designed a novel photoelectrocatalytic (PEC) system for the efficient conversion of SO_2 and NO_x in mixed gases and NO_x^- and SO_3^{2-} in wastewater to N_2 and SO_4^{2-}, respectively, by activating SO_3^{2-} to form $SO_3\bullet^-$. The key ideas include the conversion of SO_3^{2-} from SO_2 and efficient activation of SO_3^{2-} into $SO_3\bullet^-$ and further conversion into $SO_4\bullet^-$ by the MoS_2/Fe_2O_3 photoanode. Simultaneously, NO_3^-/NO_2^- originating from NO_x was rapidly reduced to NH_4^+ on the CuNW@CF cathode. Ultimately, the generated NH_4^+ was selectively oxidized to N_2 by $SO_4\bullet^-$ and $SO_4\bullet^-$ was reduced to SO_4^{2-}. The results indicated that 99.9 % of TN was removed and 100 % of SO_3^{2-} was converted to harmless SO_4^{2-}. This study provides new insights into the treatment of sulfurous and nitrogenous oxides in air and water.

1. Introduction

Sulfurous and nitrogenous oxides, including NO_x and SO_2, and the generated substances NO_x^- and SO_3^{2-} widely exist in air and water as pollutants, and they are difficult to control in the environment. Industrial activities, including fuel combustion, iron and steel smelting, and oil refining generate acidic gases, such as nitric oxides (NO_x) and sulfur dioxide (SO_2) [1–3]. Furthermore, the food and electroplating industries discharge large amounts of sulfite (SO_3^{2-}) and nitrite/nitrate (NO_x^-) [4], which the concentration of N (nitrate) and of S (sulfite) are 12–250 mg/L and more than 200 mg/L, separately [5–7]. Although selective catalytic reduction (SCR) and limestone wet treatment have high efficiency for NO_x and SO_2 removal [8–10], their complicated treatment and high running costs are unfavorable for small-scale applications [11]. In particular, more than 800,000 small- and medium-sized coal-fired boilers and industrial furnaces operate in China, and they cannot be simultaneously equipped with wet flue gas desulphurization (WFGD) and NH_3-SCR treatment technology because of the huge associated costs [11]. In addition, SO_3^- oxidation is critical for the further desulfurization and denitrification treatments because it is related to the purification of flue gas and utilization of the end products, while the drawbacks associated with SO_3^- oxidation are still observed [12]. In addition, high nitrate levels (including NO_2^- and NO_3^-) in water lead to eutrophication and even threaten human health, and the conversion of NO_x^- to N_2 has drawn considerable attention [13]. The simultaneous removal technologies for S and N oxide compounds from air and water is desirable for small- and medium-sized industrial production units because of increasing environmental pressure. To date, biological treatment, membrane separation, and electrochemical technologies have been applied as removal technologies [14–16]. However, the extreme environmental conditions used in these technologies restrict the survival of microorganisms, resulting in inefficient biological treatments [17]. In addition, the high cost of membranes restricts the large-scale use of membrane separation [18]. Additionally, the

* Corresponding authors at: School of Environmental Science and Engineering, Key Laboratory of Thin Film and Microfabrication Technology (Ministry of Education), Shanghai Jiao Tong University, Shanghai 200240, PR China.
E-mail addresses: lijinhua@sjtu.edu.cn (J. Li), zhoubaoxue@sjtu.edu.cn (B. Zhou).

https://doi.org/10.1016/j.apcatb.2023.122579
Received 27 April 2022; Received in revised form 14 February 2023; Accepted 3 March 2023
Available online 6 March 2023

reduction products of nitrates are not easily processed by electrochemical technology [19] because directly converting NO_3^- to nitrogen (N_2) is difficult [20]. Unfortunately, effective and environmentally friendly methods have not been found to remove NO_x^-.

Recently, photoelectrocatalytic (PEC) technology for pollutant removal has been intensively studied because this technology can utilize solar energy to generate reactive oxides in situ without the addition of chemicals [21–25]. For example, our previous work confirmed that the conversion of NO_3^- to N_2 was achieved by in situ activation of chloride ions to generate chlorine radicals (Cl•) [23,26]. However, the PEC activation of chloride ions to generate Cl• inevitably produces toxic by-products, such as chlorate (ClO_3^-) and perchlorate (ClO_4^-) ions [27–29], which is a serious problem in water purification.

Inspiringly, researchers have reported that SO_3^{2-} conversion can be catalyzed using transition metals (Mn, Co, Mo, or Fe) to generate sulfite free radicals ($SO_3^{\bullet-}$) and then further converted to sulfate free radicals ($SO_4^{\bullet-}$) [30–34]. Meanwhile, $SO_4^{\bullet-}$ possesses excellent oxidizing ability with standard reduction potential of 2.5–3.1 V vs. NHE, and it has a preeminent oxidative hydrogen abstraction capability and can selectively oxidize NH_4^+ to N_2 as it is converted into SO_4^{2-} [35]. Zhang et al. reported that a MoS_2/TiO_2 photoanode can capture SO_3^{2-} to form $SO_x^{\bullet-}$ ($SO_3^{\bullet-}$ and $SO_4^{\bullet-}$), and the formed radicals can selectively oxidize NH_4^+ to N_2 [21]. Notably, replacing reactive chlorine species with $SO_4^{\bullet-}$ can effectively prevent the production of toxic chlorate (e.g., ClO_3^- and ClO_4^-) [36,37]. Evidently, this is not only of great significance in denitrification treatment but it can also be used to convert harmful SO_3^{2-} in water bodies to harmless SO_4^{2-}. Importantly, according to published papers, NO_3^- can be efficiently reduced to NH_4^+ using modified copper foam [19,26,38,39]. Hence, combining the above two ideas can solve the problem of NO_3^- being selectively converted to N_2 in an environmentally friendly manner. In addition to the formed ionic NO_3^- and SO_3^{2-}, the designed PEC system also comprehensively treats acid gas mixed with NO_x and SO_2. Hence, a gas absorber was added in front of the constructed PEC system to broaden the practical applicability, thereby ensuring the efficient treatment of homogeneous waste gas and wastewater.

A novel dual-function PEC system was constructed to efficiently convert SO_2 and NO_x in waste gas and SO_3^{2-} and NO_x^- in wastewater to SO_4^{2-} and N_2, respectively. Meanwhile, SO_3^{2-} obtained from the environment or from NaOH absorption was first oxidized efficiently into $SO_3^{\bullet-}$ on the MoS_2/Fe_2O_3 photoanode, in which the MoS_2/Fe_2O_3 photoanode with superior alkali corrosion resistance showed excellent ability to induce SO_3^{2-} to form $SO_4^{\bullet-}$ under light irradiation [30,40,41]. Copper nanowire-decorated copper foam (CuNW@CF) cathodes have an outstanding capacity to reduce NO_x^- to NH_4^+ because of their large surface area and substantial number of Cu active sites. Ultimately, NH_4^+ in the system is selectively oxidized to N_2 by $SO_4^{\bullet-}$ and $SO_4^{\bullet-}$ is eventually reduced to SO_4^{2-}. This study offers new insights into the treatment of waste gas or wastewater containing NO_x and SO_2 via a simple and safe method.

2. Materials and methods

2.1. Chemicals and reagents

Fluorine-doped tin oxide (FTO, 13 Ω cm^{-1}) and copper foam (CF, 1 mm thick) were purchased from Nippon Sheet Glass Co., Ltd., China., and Suzhou Taili Metal Foam Co., Ltd., China. Analytical reagent grade $NaNO_3$, $NaNO_2$, $(NH_4)_2SO_4$, Na_2SO_3, and NaOH were obtained from Sinopharm Chemical Reagent Co. Ltd., China. Tert-butanol (TBA), thiourea, and dimethyl pyridine N-oxide (DMPO) were obtained from Aladdin Industrial Corporation. Milli-Q ultrapure water was used to produce deionized (DI) water. High-purity compressed gases (NO, NO_2, SO_2, CO_2, O_2, and N_2) were purchased from Air Liquide Co., Ltd., Shanghai, China.

2.2. Electrode preparation

The MoS_2/Fe_2O_3 photoanode was prepared in two steps (Figure. S1) [42,43]. First, Fe_2O_3 nanorods were grown on FTO via a hydrothermal method. Then, MoS_2 nanoclusters were further fabricated on the prepared Fe_2O_3 nanorods via a hydrothermal method. Finally, the prepared MoS_2/Fe_2O_3 was washed with deionized (DI) water and dried at 60 °C under vacuum. The CuNW@CF cathode was prepared by in situ wet-chemical oxidation and electrochemical reduction [44]. The details of the MoS_2/Fe_2O_3 photoanode and CuNW@CF cathode preparation are provided in the Supplementary materials.

2.3. Analytic methods

The gases produced from the constructed system, including NO, NO_2, N_2, and SO_2, were analyzed using an on-line GC system (Fuli Instruments, 9790Plus, Taizhou, China). The concentrations of ions containing SO_3^{2-} and SO_4^{2-} were confirmed via ion chromatography (MIC, METROHM, Switzerland), and the standard colorimetric method was performed using a UV–visible spectrophotometer (752N, INESA, Shanghai, China) to determine the concentrations of NO_3^-, NH_4^+ and NO_2^-. The respective calibration curves are shown in Fig. S2. A Multi N/C 3100 TOC/TN analyzer (Analytikjena, Germany) was used to determine the TN concentration. Electron spin resonance spectroscopy (ESR, Micro ESR, USA) was used to determine the free radicals. Different types of electrodes were used in the CHI 660E electrochemical analyzer to compare the photoelectric activity, including the linear sweep voltammetry (LSV) and electrochemical impedance spectroscopy (EIS). X-ray diffraction (XRD, Rigaku D-Max B), field-emission scanning electron microscopy (FE-SEM, Zeiss SUPRA55-VP), and X-ray photoelectron spectroscopy (XPS, AXIS UltraDLD) were used to determine the phases and crystallinity (XRD), morphology and elemental composition (FE-SEM), and chemical state (XPS) of the prepared electrodes.

2.4. Degradation experiment

The constructed PEC reactor was implemented in a single quartz reactor with a conventional three-electrode configuration, in which CuNW@CF was the working electrode (2.5 × 4 cm^2), MoS_2/Fe_2O_3 was the counter electrode (2.5 × 4 cm^2), and Ag/AgCl was the reference electrode. The constructed system was operated using an electrochemical workstation under irradiation (100 mW cm^{-2}) using a 350 W Xe lamp (Perfect, China) in a single chamber. Moreover, we equipped a closed-reactor device to determine the amount of gas produced. Different NO: NO_2 ratios and variable concentrations of SO_2 were dissolved in NaOH solution to simulate the lye absorption of waste liquid under different exhaust gas conditions. The electrolyte solutions were 0.1 M NaOH solutions with different concentrations of SO_3^{2-}, NO_2^-, and NO_3^-. H_2SO_4 (5 M) was used to adjust the initial pH of the simulated solution.

2.5. Construction of the gas absorption device

The gas absorption device placed before the PEC system is shown in Fig. S3. First, the N_2 gas cylinder was opened to circulate the gas circuit and then closed. Next, the flow of SO_2 was controlled by the pressure-reducing valve, the SO_2 gas cylinder was closed, and NO_2 and NO were introduced. Finally, different acidic gases were absorbed by pumping into a sodium hydroxide (NaOH) solution. After the complete absorption of exhaust gases, the waste liquid (containing SO_3^{2-}, NO_3^-, and NO_2^-) flowed into the PEC reactor. Finally, both NO_x and SO_2 were converted to harmless N_2 and SO_4^{2-} in the body of the PEC reactor.

2.6. Experiment and data-processing method

The removal experiments were conducted in a single quartz reactor

(specification 100 mL: the volume of the added solution was 80 mL). The distance between the anode and cathode was maintained at 3 cm, and the immersion areas of the cathode and anode were both 5 cm^2 (2.5 cm × 2 cm), in which the applied potential was −1.4 V vs. Ag/AgCl. Furthermore, the simulated solution containing 30 mg/L TN (different rate of NO_3^-: NO_2^-), 0.02 M SO_3^{2-}, and 0.1 M NaOH were used in the experiments. The removal rate was calculated based on the following equation.

$$\text{Removal rate} = (C_0\text{-}C_t)/C_0 \times 100\ \% \quad (1)$$

where C_0 is the initial concentration and C_t is concentration at t-time.

The conversion between the potentials vs. Ag/AgCl and vs. RHE was performed using the following equation:

$$E\ (\text{vs·RHE}) = E\ (\text{vs·Ag/AgCl}) + 0{\cdot}199\text{V} + 0{\cdot}0591\text{V} \times \text{pH} \quad (2)$$

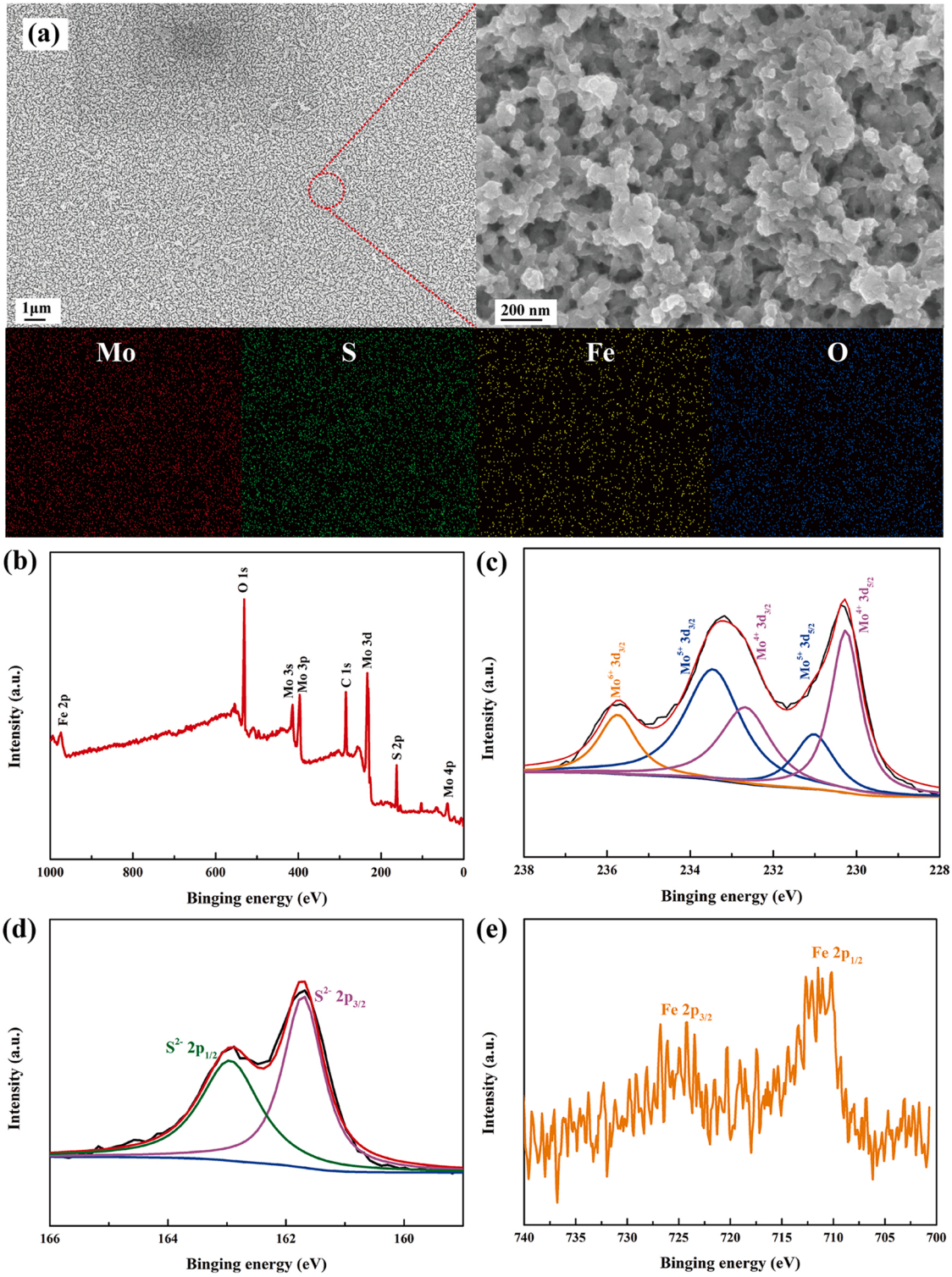

Fig. 1. (a) scanning electron microscope (SEM) image and element mapping of the MoS_2/Fe_2O_3. (b) X-ray photoelectron spectroscopy (XPS) patterns of MoS_2/Fe_2O_3 electrode; (c-e) Mo 3d peak, S 2p peak and Fe 2p peak of MoS_2/Fe_2O_3 electrode.

3. Results and discussion

3.1. Characterization of CuNW@CF cathode

Figs. S4a and S4b display SEM images of CuNW@CF, in which the modified CuNWs (approximately 50–150 nm in diameter) were coated on the copper foam. The XRD results (Fig. S4c) showed diffraction peaks representative of metallic Cu at 43.3°, 50.4°, and 74.1° [39]. Moreover, as shown in Fig. S4d, the Cu 2p spectrum contained two peaks at 931.8 and 934.4 eV, and comparing the intensities of these two peaks indicated that the main nanowires were converted to pure copper [38].

3.2. Characterization of MoS_2/Fe_2O_3

FE-SEM was used to investigate the morphology and elemental distribution of the MoS_2/Fe_2O_3 anode (Fig. 1**a**). As shown in Fig. 1**a**, after the two-step process, Fe_2O_3 nanorods (Fig. S5) grown on FTO were evidently covered with MoS_2 nanoclusters, among which the sizes of the MoS_2 nanoclusters were approximately 100 nm. In addition, the electrochemical active surface area (ECSA) of the MoS_2/Fe_2O_3 photoanode was evaluated using the electrochemical double-layer capacitances (Fig. S6), in which the active surface area increased to 2 cm^{-2}. Elemental mapping confirmed the elemental distributions of MoS_2 and Fe_2O_3. Owing to the low content of modified MoS_2, the XRD pattern did not show significant differences between the Fe_2O_3 and MoS_2/Fe_2O_3 electrodes (Fig. S7). XPS measurements were performed to confirm the elemental composition and valence state of MoS_2/Fe_2O_3. In Fig. 1**b**, characteristic peaks were observed in the total XPS spectra, which indicated that the prepared catalyst contained four elements of Mo, S, Fe, and O. Fig. 1**c** shows that the peaks at 230.2 eV and 232.7 eV were Mo^{4+} 3d, the peaks at 231.1 eV and 233.5 eV were Mo^{5+} 3d, and the peak at 235.8 eV was Mo^{6+} 3d [45]. In Fig. 1**d**, peaks located at 161.7 eV and 162.9 eV were S^{2-} $2p_{3/2}$ and S^{2-} $2p_{1/2}$ of MoS_2, respectively [45]. Additionally, Fig. 1**e** shows that the peaks located at 710.8 eV and 724.3 eV, 713.0 eV, and 727.1 eV were Fe^{2+} 2p and Fe^{3+} 2p, respectively [46]. Moreover, MoS_2/Fe_2O_3 exhibited an outstanding photocurrent density, as indicated by the LSV curves (Fig. S8a). The photocurrent density of single MoS_2 and Fe_2O_3 was 0.44 and 0.58 mA cm^{-2} at 1.23 V, respectively. Nevertheless, the photocurrent density increased to 2.22 mA cm^{-2} when MoS_2 and Fe_2O_3 were combined to fabricate the MoS_2/Fe_2O_3 electrode. The UV-Vis absorption spectra in Fig. S8b show that the absorbance of MoS_2/Fe_2O_3 was higher than that of Fe_2O_3 because the photogenerated carriers of MoS_2 are more easily excited than Fe_2O_3[47], which affects the absorption capacity. The prepared MoS_2/Fe_2O_3 electrode using the epitaxial MoS_2 layer based on band matching enhanced the surface area and facilitated interfacial charge transport owing to Fermi level matching of MoS_2 and Fe_2O_3. Hence, the fabricated MoS_2/Fe_2O_3 electrode broadened the wavelength absorption range and increased the photocurrent density.

3.3. Mechanism of sulfite radicals mediated TN removal

The probable mechanism underlying the designed PEC system is shown in Fig. 2**a**. First, sulfurous and nitrogenous oxides, including NO_x and SO_2, were absorbed into the NaOH solution to form NO_x^- (NO_3^- and NO_2^-) and SO_3^{2-} (Eqs. 3–4**)**. Detailed information on the concentrations of different pollutants is shown in Table S1. Photogenerated holes (h^+) and electrons were produced on the MoS_2/Fe_2O_3 photoanode under irradiation (Eq. 5) [21] because of the easy band gap transition and good absorption of light by MoS_2/Fe_2O_3. Meanwhile, the valence band energies (E_{VB}) of pristine MoS_2 and Fe_2O_3 are 1.78 and 2.09 eV, respectively (Figs. S9 and S10). The E_{VB} of MoS_2 was higher than that of Fe_2O_3, thus forming a heterojunction. In addition, both MoS_2 and Fe_2O_3 absorbed photons to generate charge carriers under illumination, and the electrons in the conduction band (CB) of MoS_2 flowed into the CB of Fe_2O_3 and were then injected into FTO to flow to the CuNW@CF to reduce NO_x^-. The holes generated in the valence band (VB) of Fe_2O_3 flowed into the VB of MoS_2 to effectively oxidize SO_3^{2-} (Eq. 6) [48]. Thereafter, $SO_3^{\bullet-}$ was further oxidized to $SO_5^{\bullet-}$ and $SO_4^{\bullet-}$ (Eqs. 7–8) [32, 35,49]. Simultaneously, NO_3^- was easily adsorbed on the CuNW@CF cathode (Eq. 9) [19] and converted to NO_2^- (Eq. 10) [19]. Similarly, NO_2^- was also adsorbed on the CNW@CF cathode (Eq. 11) [19] and further rapidly reduced to NH_4^+ (Eq. 12) [19] because the modified CuNWs provided more abundant active sites, which accelerated the reduction reaction of NO_x^- [19,50]. To confirm this assertion, the ECSA of CF and CuNW@CF were measured, and the results are shown in Fig. S11. The ECSA (12.8 cm^{-2}) was dramatically increased after the modification of CuNWs, and the value of CuNW@CF was 4.2 times greater than that of pure CF. Moreover, $SO_3^{\bullet-}$ and $SO_5^{\bullet-}$ were converted to $SO_4^{\bullet-}$, which dominated the oxidation of NH_4^+. Ultimately, NH_4^+ was completely oxidized to N_2 and $SO_4^{\bullet-}$ was converted to SO_4^{2-} after a series of reactions (Eqs. 13–16) [21,48], which realized the efficient removal of NO_x and SO_2 simultaneously. Notably, NO_3^- was first reduced to NO_2^-, which resulted in an increase in NO_2^- during the initial 10 min (Fig. S12a). Finally, TN was effectively converted into N_2, and all the toxic SO_3^{2-} was efficiently transformed into non-toxic SO_4^{2-}. In total, 99.9 % N_2 and 100 % SO_4^{2-} were generated (Fig. 2**b**). In addition, as the reaction progressed, the pH increased slowly and finally reached 12.67 because more OH^- was generated in the entire reaction (eqs 17, 18) (Fig. S12b).

$$2NO_2 + 2OH^- \rightarrow NO_2^- + NO_3^- + H_2O \quad (3)$$

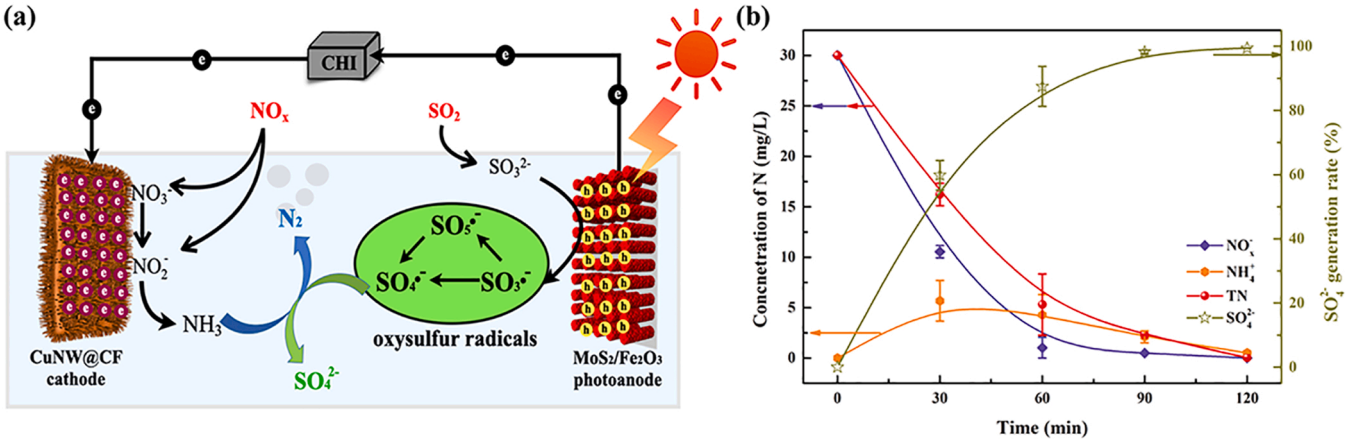

Fig. 2. (a) schematic illustration of the mechanism of the constructed PEC system; (b) the variation of NO_x^-, NH_4^+, TN (left Y axis) and SO_4^{2-} (right Y axis) in the constructed system during the reaction. Condition: SO_3^{2-} 20 mmol/L, pH = 12, TN (15 mg/L NO_2^- and 15 mg/L NO_3^-), potential − 1.4 V vs Ag/AgCl.

$$SO_2 + 2OH^- \rightarrow SO_3^{2-} + H_2O \quad (4)$$

$$MoS_2/Fe_2O_3 + h\nu \rightarrow h^+ + e \quad (5)$$

$$SO_3^{2-} + h^+ \rightarrow SO_3\bullet^- \quad (6)$$

$$SO_3\bullet^- + O_2 \rightarrow SO_5\bullet^- \; k = 1{\cdot}0\text{–}2{\cdot}5 \times 10^9\ M^{-1}\ s^{-1} \quad (7)$$

$$SO_5\bullet^- + SO_3^{2-} \rightarrow SO_4\bullet^- + SO_4\bullet^- \; k = (10^4 - 10^7)\ M^{-1}\ s^{-1} \quad (8)$$

$$NO_3^- + CuNW \rightarrow CuNW\text{-}NO_{3ads}^- \quad (9)$$

$$CuNW\text{-}NO_{3ads}^- + H_2O + 2e \rightarrow CuNW\text{-}NO_{2ads}^- + 2OH^- \quad (10)$$

$$NO_2^- + CuNW \rightarrow CuNW\text{-}NO_{2ads}^- \quad (11)$$

$$CuNW\text{-}NO_{2ads}^- + 5\ H_2O + 6e \rightarrow NH_4^+ + CuNW + 7OH^- \quad (12)$$

$$NH_4^+ + SO_4\bullet^- \rightarrow \bullet NH_2 + SO_4^{2-} + H^+ \; k = 3{\cdot}0 \times 10^5\ M^{-1}\ s^{-1} \quad (13)$$

$$\bullet NH_2 + SO_4\bullet^- \rightarrow \bullet NH + SO_4^{2-} + H^+ \quad (14)$$

$$\bullet NH + SO_4\bullet^- \rightarrow \bullet N + SO_4^{2-} + H^+ \quad (15)$$

$$\bullet N + \bullet N \rightarrow N_2 \quad (16)$$

To further confirm the removal effect of the anode on the radicals generated for TN, different anodes were used for comparison. Fig. S13 shows the removal of TN via Fe_2O_3, MoS_2, and MoS_2/Fe_2O_3. The removal reaction obeyed first-order kinetics, and 40.68 % and 69.39 % of TN were removed for Fe_2O_3 and MoS_2, respectively, which had rate constants of 0.0069 and 0.0102 min^{-1}, respectively. As for MoS_2/Fe_2O_3, approximately 99.9 % of TN was decomposed in 120 min, and the rate constant (0.0294 min^{-1}) was 4.3 times and 2.9 times greater than that of Fe_2O_3 and MoS_2, respectively. Since $SO_4\bullet^-$ can selectively oxidize NH_4^+ into N_2 when the $SO_4\bullet^-$ generated on both Fe_2O_3 and MoS_2 was insufficient, the formation of a type II heterojunction of the MoS_2/Fe_2O_3 electrode was proposed using epitaxial growth of the MoS_2 based on band matching. This process improved the photocurrent, resulting in the generation of $SO_4\bullet^-$ on MoS_2/Fe_2O_3. Finally, $SO_4\bullet^-$ converts NH_4^+ into N_2 and achieves efficient denitrification. Hence, MoS_2/Fe_2O_3 showed the best performance compared to Fe_2O_3 and MoS_2 electrodes.

3.4. Removal performance of the photoelectrocatalytic system

To reveal the performance of the novel PEC system, we compared different catalytic systems, and the results are displayed in Figs. S14, S15, and 3. SO_3^{2-} was completely converted into SO_4^{2-} in the PEC system, and the generation rate (0.044 min^{-1}) was 11.0 times and 3.4 times higher than that of the photocatalytic (PC) (0.004 min^{-1}) and electrocatalytic (EC) (0.013 min^{-1}) systems, respectively. In addition, Fig. S15 shows that the tendencies of NO_3^- reduction in EC and PEC were basically the same: all NO_3^- was reduced in 120 min while only 7.1 mg/L of NO_3^- was reduced in the EC system, which is because NO_x^- reduction should

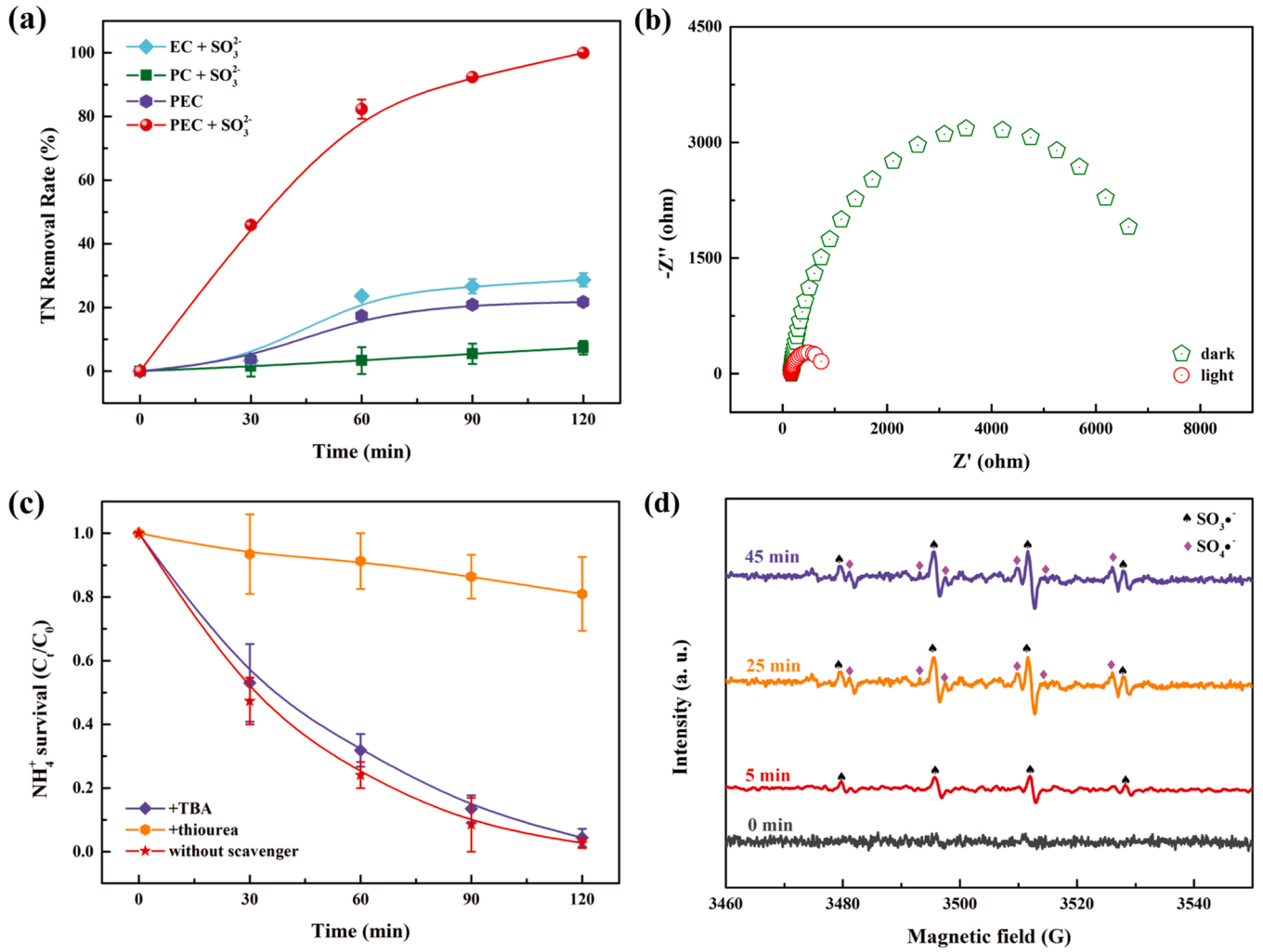

Fig. 3. (a) TN (15 mg/L NO_2^- and 15 mg/L NO_3^-) removal versus time by electrocatalytic-sulfite, photocatalytic-sulfite, phtoelectrocatalytic and phtoelectrocatalytic-sulfite systems; (b) electrochemical impedance spectroscopy (EIS) analysis of MoS_2/Fe_2O_3 in different conditions; (c) the experiments of NH_4^+ degradation with different scavenger; (d) electron spin-resonance spectroscopy (ESR) spectra in phtoelectrocatalytic and phtoelectrocatalytic-sulfite systems.

overcome high kinetic barriers [51]. Fig. 3**a** shows the TN removal rate in different systems. The PC system showed poor TN removal capability, in which only 7.4 % of TN was removed in 120 min and 14.4 mg/L of NO_3^- and 13.0 mg/L of NO_2^- remained (Fig. S16). Almost all NO_x^- was reduced to NH_4^+ (21.6 mg/L) via the EC system, resulting in 28.7 % of TN was degraded because the PC system cannot overcome the reduction barrier of NO_x^- compared to the EC system. In addition, we tested the performance of a PEC system without SO_3^{2-} that achieved 21.8 % TN removal, in which NH_4^+ was directly oxidized by the MoS_2/Fe_2O_3 photoanode [52]. In addition, 18.3 mg/L NH_4^+ and 5.1 mg/L NO_2^- (Fig. S16) remained after 120 min. However, the PEC system with SO_3^- showed a predominant performance for TN removal, in which 99.9 % of TN was discomposed without any nitrogen compound residues. Compared with PC and EC systems, MoS_2/Fe_2O_3 of PEC can very effectively generate h^+ under irradiation and directly oxidize SO_3^{2-} on the surface to generate $SO_3\bullet^-$ and further form $SO_4\bullet^-$. In addition, owing to the effect of the external electrical energy, the electrons are directly transferred to the cathode to reduce NO_x^- to NH_4^+, thereby effectively inhibiting the recombination of electrons and holes generated in MoS_2/Fe_2O_3 and finally breaking the limitations of PC and EC in mass transfer. Subsequently, the generated $SO_4\bullet^-$ selectively oxidizes NH_4^+ to N_2 to achieve TN removal [35]. Notably, the reaction combining SO_3^{2-} oxidation and NO_x^- reduction is a thermodynamically spontaneous process (eqs. 17,18).

$$2NO_2^- + 3SO_3^{2-} + H_2O \rightarrow N_2 + 3SO_4^{2-} + 2OH^- \quad (17)$$

$$\Delta G = -1083.84 \text{ kJ mol}^{-1}$$

$$2NO_3^- + 5SO_3^{2-} + H_2O \rightarrow N_2 + 5SO_4^{2-} + 2OH^- \quad (18)$$

$$\Delta G = -744.28 \text{ kJ mol}^{-1}.$$

Hence, the PEC-sulfite system improved the rate constant of TN removal to 0.0294 min^{-1}, which was 12.8 times, 42.0 times, and 9.2 times higher than that of the pure PEC, PE-sulfite, and EC-sulfite systems, respectively (Fig. S17a). Because the photoanodic catalytic activation of SO_3^{2-} to $SO_3\bullet^-$ determines the denitrification ability, we explored the electrochemical impedance spectroscopy (EIS) Nyquist analysis of light on the anodic charge transport in the PEC-sulfite system, where the diameter of the fitted semicircle represents the charge transfer resistance, which is inversely proportional to the rate of charge transfer in the MoS_2/Fe_2O_3 anode. In the Nyquist plot shown in Fig. 3**b**, the MoS_2/Fe_2O_3 system under light had a much narrower semicircle diameter than that in the dark, indicating that the resistance to carrier migration under illumination was decreased. However, both light and SO_3^{2-} mainly involved anode reactions, in which the charge transfer behavior of CuNW@CF displayed no evident change (Fig. S18). The active ingredients of the constructed system were further investigated based on the performance of the PEC–sulfite system. First, a series of experiments using different radical scavengers was performed to exclude the interference of other possible oxidant species. Tert-butyl alcohol (TBA) quenching of OH• was used to demonstrate the role of OH•, whereas thiourea can remove both OH• and $SO_x\bullet^-$ [49,53]. As shown in Figs. 3**c** and **S17b**, the NH_4^+ removal performance of thiourea dramatically decreased, with a removal rate constant of 0.0017 min^{-1}. On the contrary, the NH_4^+ removal performance with TBA showed no evident change compared with the condition without the addition of the scavenger (0.0254 min^{-1}). The results in Figs. 3**c** and **S17b** illustrated the absence of OH• and the key role of $SO_x\bullet^-$ in TN removal. ESR was used to detect radical species. In Fig. 3**d**, an clear peak was not observed before the PEC-sulfite system booted, whereas the same characteristic peak as the standard peak of $SO_3\bullet^-$ appeared (provided by Bruker Biosciences Corporation, Fig. S19a) after 5 min of reaction. Moreover, as the PEC-sulfite reaction continued, the characteristic peaks of $SO_3\bullet^-$ and $SO_4\bullet^-$ appeared together (reaction time: 25 and 45 min, respectively), which indicated that $SO_3\bullet^-$ was further converted into $SO_4\bullet^-$. However, clear characteristic peaks were not observed when thiourea was added to the PEC-sulfite system (Fig. S19b), which further confirmed that $SO_4\bullet^-$, sourced from $SO_3\bullet^-$ and $SO_3\bullet^-$, played a key role in denitrification.

3.5. Effect of the applied potential

The applied potential significantly affects the reduction of NO_x^-, the results of which are shown in Figs. 4**a** and **S20a**. The TN removal rate increased as the applied potential increased. For example, 54.0 % of TN was removed at −0.1 V, and 1.6 mg/L NO_3^-, 11.4 mg/L NO_2^-, and 0.8 mg/L NH_4^+ remained; however, 71.9 % of TN was removed at −0.3 V and only 8.0 mg/L NO_2^- remained. With further improvements in the applied potential, almost all TN was removed (more than 99 %) and no other nitrogen compounds were detected (below the detection limit). The enhancement in TN removal was attributed to the occurrence of NO_x^- reduction at a higher potential. Additionally, faradaic efficiency represents another parameter for determining the optimal applied potential. As shown in Fig. S21, the faradaic efficiency at −0.5 V was higher than that at other applied potentials because of the inhibition of hydrogen evolution. Therefore, considering both the TN removal performance and faradaic efficiency, the applied potential of −0.5 V was the most suitable condition for the PEC system.

3.6. Effect of the initial pH

Because lye was used in the process of absorbing acid gas, the absorbing liquid remained alkaline. Hence, we studied denitrification under conditions of high initial pH values (pH 8–14), and the results are displayed in Fig. 4**b**. TN removal remained high at different pH values: 93.2 %, 99.2 %, 99.9 %, and 99.9 % of TN were removed, which corresponded to pH values of 8, 10, 12, and 14, respectively. Moreover, except at pH 8 (1.4 mg/L NH_4^+ remained), no nitrogen compounds were detected after the reaction (Fig. S20b) because $SO_3\bullet^-$ is easily generated under alkaline conditions, which converts NH_4^+ to N_2, resulting in efficient TN removal [54]. Therefore, with a high pH value, no NH_4^+ residual or TN were removed. Thus, a pH of 12 was selected for the simulated wastewater.

3.7. Effect of SO_3^{2-} concentration

SO_3^{2-} can not only promote the reduction of NO_x^- but can also be used as a raw material to produce $SO_4\bullet^-$, which achieves efficient denitrification. Therefore, different concentrations of SO_3^{2-} were added to the PEC system to verify its effectiveness. As shown in Fig. 4**c**, TN removal was influenced by the concentrations of SO_3^{2-}, in which the removal rate of TN increased as the concentration of SO_3^{2-} increased. When no SO_3^{2-} was added, only 21.7 % of TN was removed and 9.3 mg/L NO_2^- and 14.0 mg/L NH_4^+ remained in system (Fig. S20c) because NH_4^+ can be oxidized by transition metals under alkaline conditions[52]. As the amount of added SO_3^{2-} continued to increase (5–25 mmol/L), the denitrification performance improved, with TN removal rates of 51.0 %, 66.7 %, 99.9 %, and 99.9 %. $SO_4\bullet^-$ was derived from SO_3^{2-} via the MoS_2/Fe_2O_3 photoanode, which dominated the conversion of NH_4^+ to N_2, resulting in a dramatic decrease in NH_4^+ residue and high TN removal. Hence, more TN was removed at a higher initial concentration of SO_3^{2-}. Correspondingly, NH_4^+ remained because the initial concentrations of SO_3^{2-} was lower than 20 mM (Fig. S20c**)**, which failed to generate sufficient $SO_4\bullet^-$ for the selective conversion of NH_4^+.

3.8. Effect of the ratio of NO_2^-: NO_3^-

Different ratios of NO_2^-: NO_3^- were formed during the absorption of NaOH for NO_x. Hence, the performance of the PEC system was tested because different ratios of NO_2^-: NO_3^- waste liquid may be formed during the spray absorption process. As shown in Fig. 4**d**, all ratios of NO_2^-: NO_3^- could be efficiently degraded in 120 min, and all types of nitrogen-containing compounds were lower than the detection value (Fig. S20d), which showed extremely similar tendencies. Cu nanowires

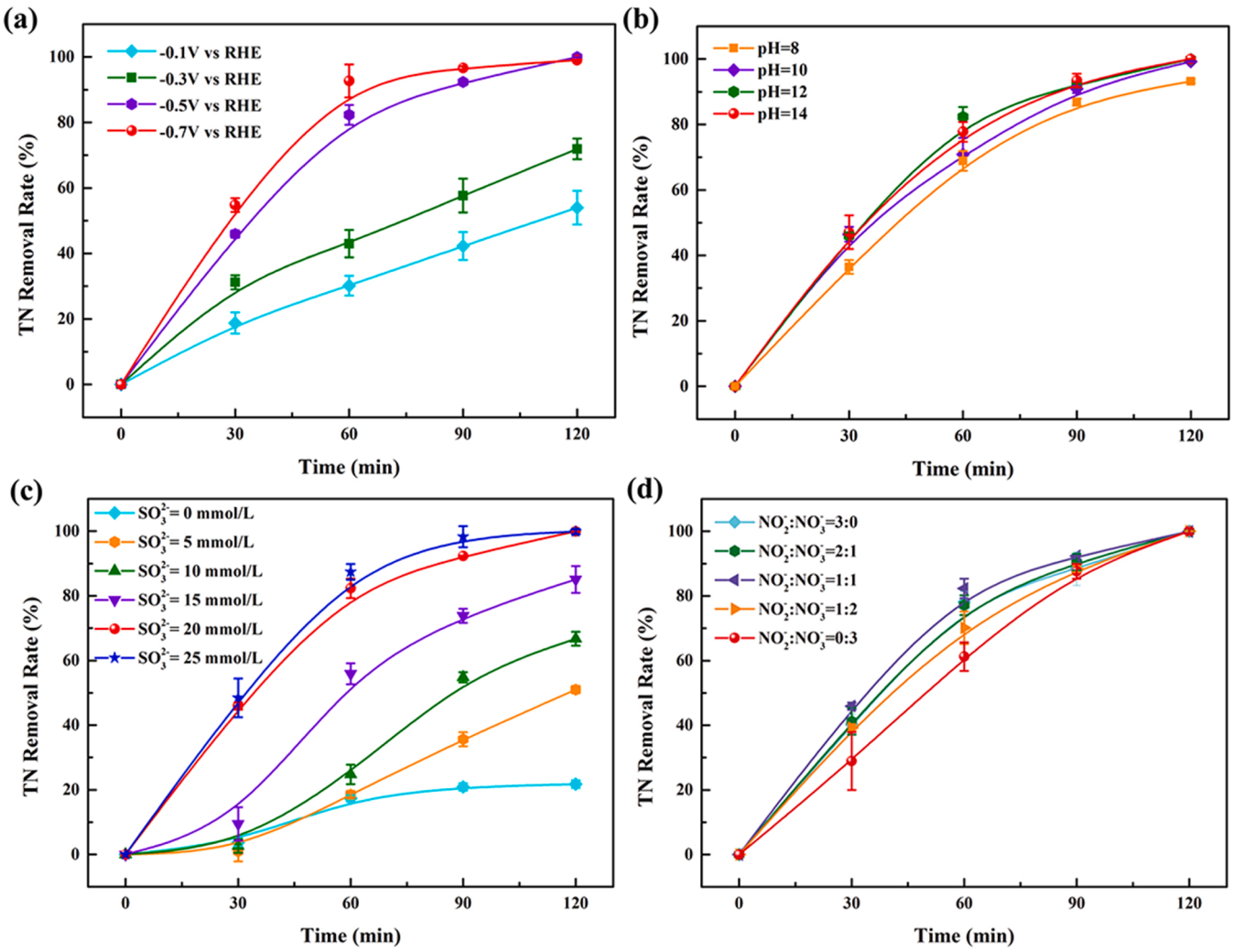

Fig. 4. Effect of (a) applied potential (vs RHE), (b) initial pH, (c) SO_3^{2-} concentration and (d) ratio of NO_2^-:NO_3^- on TN removal. TN: 15 mg/L NO_2^- and 15 mg/L NO_3^-.

with abundant active sites displayed excellent ability to reduce NO_x^-, in which both NO_3^- and NO_2^- were effectively converted to NH_4^+ [19,26,38]. Simultaneously, $SO_4^{\bullet-}$ generated by the MoS_2/Fe_2O_3 photoanode further oxidized the generated NH_4^+ into N_2, thus realizing the efficient removal of TN. In summary, the constructed PEC system was feasible for treating wastewater with different compositions of NO_x^- and showed remarkable denitrification performance.

The specific conversion of SO_2 to non-toxic SO_4^{2-} can be divided into

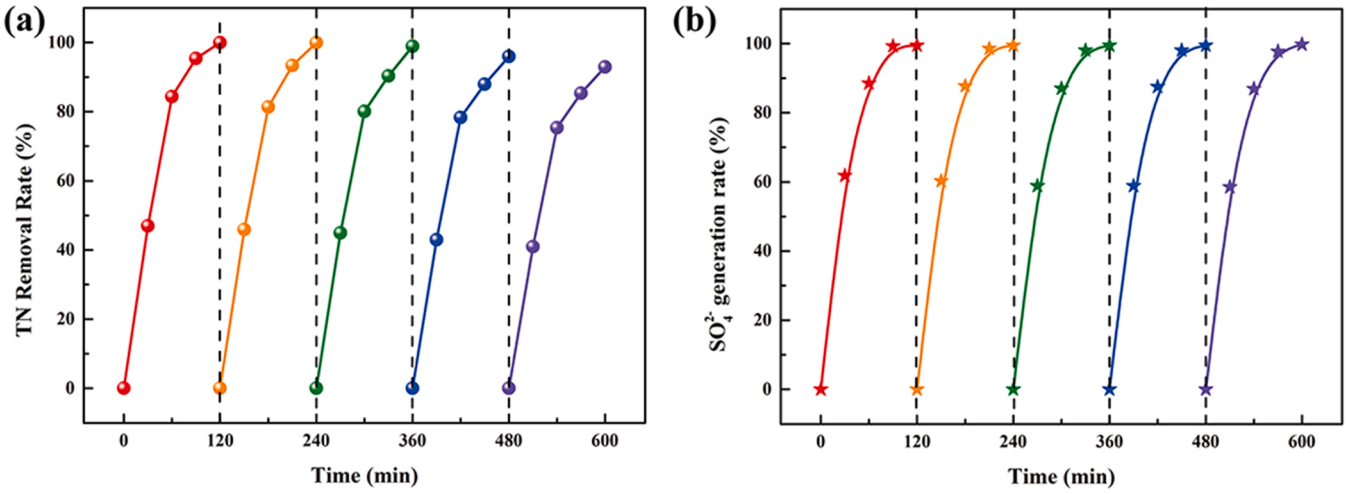

Fig. 5. (a) removal of TN and (b) SO_4^{2-} generation in PEC system during five tests at 120 intervals. Condition: SO_3^{2-} 20 mmol/L, pH = 12, TN (15 mg/L NO_2^- and 15 mg/L NO_3^-), potential −1.4 V vs Ag/AgCl.

two steps: absorption and PEC reaction. First, SO_2 was absorbed by NaOH solution and converted to SO_3^{2-}. Then, h^+ was generated on MoS_2/Fe_2O_3 under light irradiation and captured by SO_3^{2-} adsorbed onto the active sites of MoS_2/Fe_2O_3 to form $SO_3\bullet^-$ and $SO_4\bullet^-$ (Eqs. 6–8). Meanwhile, $SO_4\bullet^-$ was rapidly captured by NH_4^+, and oxidized to SO_4^{2-} (Eqs. 13–15). Although dissolved oxygen was rare in the solution, SO_3^{2-} could partially react with dissolved O_2 to form SO_4^{2-}. However, compared with NO_x^- reduction, which should overcome the high kinetic barriers [51], SO_3^{2-} could more easily convert to SO_4^{2-} via PEC, in which SO_3^{2-} was completely transformed into SO_4^{2-} under different conditions (Table S2). Hence, we mainly discuss denitrification under different conditions.

3.9. Stability and application

The catalytic stability and selectivity of the photoanode and cathode are critical for further application. Thus, additional tests were performed to study catalytic stability and selectivity. As shown in Fig. 5, the TN removal rates in the five tests were 99.9 %, 99.9 %, 98.9 %, 95.9 %, and 92.9 %, which were maintained at high levels (Fig. 5**a**). The SO_4^{2-} generation rate in the five tests was maintained above 99 % (Fig. 5**b**). Moreover, the CuNW@CF cathode was applied to reduce NO_x^- under different CO_2 concentrations, and the results showed that NO_x^- reduction trends did not change with different CO_3^{2-} concentrations (Fig. S22). To confirm the effects of other gases, experiments with exposure to different gases were conducted, and the results are shown in Fig. S23. There was no significant change in TN removal when N_2 and CO_2 were pumped. However, TN removal decreased when air and simulated flue gas were pumped because dissolved oxygen could directly oxidize SO_3^{2-} to SO_4^{2-}; thus, $SO_4\bullet^-$ production was suppressed, which further inhibited the reaction with the generated NH_4^+ and ultimately limited TN removal. Conversely, the pumping gas accelerated the mixing of ions in the solution; thus, the rates of SO_4^{2-} generation were accelerated. In addition, to broaden the practical application value of the PEC system, we collected spray tower treatment wastewater (details are described in Table S3) as the treatment object, and the results are shown in Fig. 6. SO_3^{2-} and TN were both decomposed within 5 h (99.4 % of SO_3^{2-} and 95.4 % of TN, respectively). After treatment via the PEC system, both the chemical oxygen demand (COD) and total nitrogen (TN) (containing NO_3^- and NH_4^+) were lower than 15 and 0.5 mg/L, respectively, which meet the environmental quality standards for surface water (**GB 3838–2002**) and indicate the great potential for the practical application of PEC systems. For practical applications in combustion equipment, this technology can convert both NO_x and SO_2 from flue gas into non-toxic and harmless N_2 and SO_4^{2-} at room temperature, which means that the reaction conditions of this technology are mild and will not produce secondary pollution. As for desalination of wastewater, considering the huge difference in the solubility of Na_2SO_4 and NaOH, evaporative crystallization is promising for Na_2SO_4 recovery using this technology [55].

4. Conclusion

This study offers new insights into the simultaneous removal of both SO_2 and NO_x from waste gas and SO_3^{2-} and NO_x^- from wastewater based on sulfite activation by PEC reaction, in which 99.9 % of TN is removed and 100 % of SO_3^{2-} is converted to harmless SO_4^{2-} in 120 min. Meanwhile, the TN removal rates were 42.0 times and 9.2 times higher than that of the PC and EC systems, respectively, and the SO_4^{2-} generation rates were 11.0 times and 3.4 times higher than that of the PC and EC systems, respectively. In addition, ESR experiments revealed the functions of $SO_3\bullet^-$ and $SO_4\bullet^-$. In the PEC system, the main reactive species were $SO_3\bullet^-$ and $SO_4\bullet^-$, which resulted in a high TN removal rate under alkaline conditions, while $SO_3\bullet^-$ was the initiator, thus leading to $SO_4\bullet^-$ formation. This study provides important technical and fundamental knowledge for the possible application of PEC treatments using sulfurous and nitrogenous oxides.

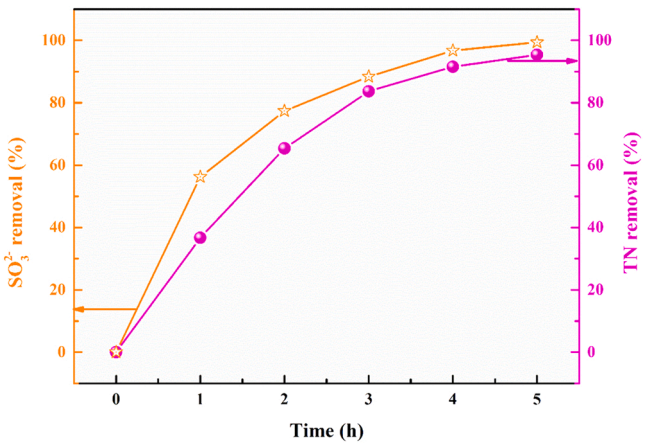

Fig. 6. The removal rate of SO_3^{2-} and TN in real spray wastewater. (Condition: 10 times diluted). Due to the large amount of suspended solids caused by the limestone-based method, the actual waste liquid is filtered before treatment.

CRediT authorship contribution statement

Changhui Zhou: Conceptualization, Data curation, Writing - original draft, Writing - review & editing. **Jinhua Li:** Visualization, Investigation, Supervision. **Yan Zhang:** Investigation, Data curation, Methodology. **Jing Bai**: Supervision. **Pengbo Wang:** Methodology. **Bo Zhang:** Methodology. **Lina Zha:** Methodology. **Mingce Long**: Supervision. **Baoxue Zhou:** Conceptualization, Supervision, Project administration, Writing - review & editing.

Declaration of Competing Interest

The authors declare that they have no known competing financial interests or personal relationships that could have appeared to influence the work reported in this paper.

Data availability

Data will be made available on request.

Acknowledgments

The authors would like to acknowledge the National Natural Science Foundation of China (No. 22206213, 22076121), the National Key Research and Development Program of China (2018YFE0122300), the Fundamental Research Funds for the Central Universities for financial support. We thank the AEMD center (SJTU) and instrumental Analysis Center (SJTU-SESE) for technical support.

Appendix A. Supporting information

Supplementary data associated with this article can be found in the online version at doi:10.1016/j.apcatb.2023.122579.

References

[1] Y. Liu, Y. Shan, Y. Wang, Novel simultaneous removal technology of NO and SO_2 using a semi-dry microwave activation persulfate system, Environ. Sci. Technol. 54 (3) (2020) 2031–2042, https://doi.org/10.1021/acs.est.9b07221.
[2] Y. Liu, J. Zhang, C. Sheng, Y. Zhang, L. Zhao, Simultaneous removal of NO and SO_2 from coal-fired flue gas by UV/H_2O_2 advanced oxidation process, Chem. Eng. J. 162 (3) (2010) 1006–1011, https://doi.org/10.1016/j.cej.2010.07.009.
[3] X. Zhou, Z. Li, T. Zhang, F. Wang, F. Wang, Y. Tao, X. Zhang, F. Wang, J. Huang, Volatile organic compounds in a typical petrochemical industrialized valley city of northwest China based on high-resolution PTR-MS measurements: Characterization, sources and chemical effects, Sci. Total Environ. 671 (2019) 883–896, https://doi.org/10.1016/j.scitotenv.2019.03.283.

[4] Z. Liu, S. Dong, D. Zou, J. Ding, A. Yu, J. Zhang, C. Shan, G. Gao, B. Pan, Electrochemically mediated nitrate reduction on nanoconfined zerovalent iron: properties and mechanism, Water Res. 173 (2020), 115596, https://doi.org/10.1016/j.watres.2020.115596.

[5] C. Gabaldon, M. Izquierdo, V. Martinez-Soria, P. Marzal, J.M. Penya-Roja, F. Javier Alvarez-Hornos, Biological nitrate removal from wastewater of a metal-finishing industry, J. Hazard. Mater. 148 (1–2) (2007) 485–490, https://doi.org/10.1016/j.jhazmat.2007.02.071.

[6] T. Yilmaz, E. Sahinkaya, Performance of sulfur-based autotrophic denitrification process for nitrate removal from permeate of an MBR treating textile wastewater and concentrate of a real scale reverse osmosis process, J. Environental Manag. 326 (2023), 116827, https://doi.org/10.1016/j.jenvman.2022.116827.

[7] C.H. Shen, G.T. Rochelle, Nitrogen dioxide absorption and sulfite oxidation in aqueous sulfite, Environ. Sci. Technol. 32 (13) (1998) 1994–2003, https://doi.org/10.1021/es970466q.

[8] Y. Liu, Z. Liu, Y. Wang, Y. Yin, J. Pan, J. Zhang, Q. Wang, Simultaneous absorption of SO_2 and NO from flue gas using ultrasound/Fe^{2+}/heat coactivated persulfate system, J. Hazard. Mater. 342 (2018) 326–334, https://doi.org/10.1016/j.jhazmat.2017.08.042.

[9] Y. Zhao, Y. Han, T. Ma, T. Guo, Simultaneous desulfurization and denitrification from flue gas by Ferrate(VI, Environ. Sci. Technol. 45 (9) (2011) 4060–4065, https://doi.org/10.1021/es103857g.

[10] C. Su, X. Ran, J. Hu, C. Shao, Photocatalytic process of simultaneous desulfurization and denitrification of flue gas by TiO_2-polyacrylonitrile nanofibers, Environ. Sci. Technol. 47 (20) (2013) 11562–11568, https://doi.org/10.1021/es4025595.

[11] Y. Liu, Q. Wang, J. Pan, Novel process of simultaneous removal of nitric oxide and sulfur dioxide using a vacuum ultraviolet (VUV)-activated $O_2/H_2O/H_2O_2$ system in a wet VUV-spraying reactor, Environ. Sci. Technol. 50 (23) (2016) 12966–12975, https://doi.org/10.1021/acs.est.6b02753.

[12] Z. Lian, C. Zhu, S. Zhang, W. Ma, Q. Zhong, Study on the synergistic oxidation of sulfite solution by ozone and oxygen: Kinetics and mechanism, Chem. Eng. Sci. 242 (2021), 116745, https://doi.org/10.1016/j.ces.2021.116745.

[13] L. Su, K. Li, H. Zhang, M. Fan, D. Ying, T. Sun, Y. Wang, J. Jia, Electrochemical nitrate reduction by using a novel Co_3O_4/Ti cathode, Water Res. 120 (2017) 1–11, https://doi.org/10.1016/j.watres.2017.04.069.

[14] Y. Chen, C. Peng, J. Wang, L. Ye, L. Zhang, Y. Peng, Effect of nitrate recycling ratio on simultaneous biological nutrient removal in a novel anaerobic/anoxic/oxic (A_2/O)-biological aerated filter (BAF) system, Bioresour. Technol. 102 (10) (2011) 5722–5727, https://doi.org/10.1016/j.biortech.2011.02.114.

[15] S.W. Van Ginkel, C.H. Ahn, M. Badruzzaman, D.J. Roberts, S.G. Lehman, S. S. Adham, B.E. Rittmann, Kinetics of nitrate and perchlorate reduction in ion-exchange brine using the membrane biofilm reactor (MBfR, Water Res. 42 (15) (2008) 4197–4205, https://doi.org/10.1016/j.watres.2008.07.012.

[16] Z. Shen, D. Liu, G. Peng, Y. Ma, J. Li, J. Shi, J. Peng, L. Ding, Electrocatalytic reduction of nitrate in water using Cu/Pd modified Ni foam cathode: high nitrate removal efficiency and N_2-selectivity, Sep. Purif. Technol. 241 (2020), 116743, https://doi.org/10.1016/j.seppur.2020.116743.

[17] W. Teng, N. Bai, Y. Liu, Y. Liu, J. Fan, W.X. Zhang, Selective nitrate reduction to dinitrogen by electrocatalysis on nanoscale iron encapsulated in mesoporous carbon, Environ. Sci. Technol. 52 (1) (2018) 230–236, https://doi.org/10.1021/acs.est.7b04775.

[18] D. Reyter, D. Belanger, L. Roue, Nitrate removal by a paired electrolysis on copper and Ti/IrO_2 coupled electrodes - influence of the anode/cathode surface area ratio, Water Res. 44 (6) (2010) 1918–1926, https://doi.org/10.1016/j.watres.2009.11.037.

[19] Y. Wang, W. Zhou, R. Jia, Y. Yu, B. Zhang, Unveiling the activity origin of a copper-based electrocatalyst for selective nitrate reduction to ammonia, Angew. Chem. Int. Ed. 59 (13) (2020) 5350–5354, https://doi.org/10.1002/anie.201915992.

[20] G.-F. Chen, Y. Yuan, H. Jiang, S.-Y. Ren, L.-X. Ding, L. Ma, T. Wu, J. Lu, H. Wang, Electrochemical reduction of nitrate to ammonia via direct eight-electron transfer using a copper–molecular solid catalyst, Nat. Energy 5 (8) (2020) 605–613, https://doi.org/10.1038/s41560-020-0654-1.

[21] X. Fan, Y. Zhou, G. Zhang, T. Liu, W. Dong, In situ photoelectrochemical activation of sulfite by MoS_2 photoanode for enhanced removal of ammonium nitrogen from wastewater, Appl. Catal. B: Environ. 244 (2019) 396–406, https://doi.org/10.1016/j.apcatb.2018.11.061.

[22] W. Zheng, L. Zhu, S. Liang, J. Ye, X. Yang, Z. Lei, Z. Yan, Y. Li, C. Wei, C. Feng, Discovering the importance of ClO* in a coupled electrochemical system for the simultaneous removal of carbon and nitrogen from secondary coking wastewater effluent, Environ. Sci. Technol. 54 (14) (2020) 9015–9024, https://doi.org/10.1021/acs.est.9b07704.

[23] Y. Zhang, J. Li, J. Bai, Z. Shen, L. Li, L. Xia, S. Chen, B. Zhou, Exhaustive conversion of inorganic nitrogen to nitrogen gas based on a photoelectro-chlorine cycle reaction and a highly selective nitrogen gas generation cathode, Environ. Sci. Technol. 52 (3) (2018) 1413–1420, https://doi.org/10.1021/acs.est.7b04626.

[24] J. Bai, B. Zhang, J. Li, B. Zhou, Photoelectrocatalytic generation of H_2 and S from toxic H_2S by using a novel BiOI/WO_3 nanoflake array photoanode, Front. Energy 15 (3) (2021) 744–751, https://doi.org/10.1007/s11708-021-0775-7.

[25] C. Zhou, J. Li, J. Wang, C. Xie, Y. Zhang, L. Li, T. Zhou, J. Bai, H. Zhu, B. Zhou, Efficient H_2 production and TN removal for urine disposal using a novel photoelectrocatalytic system of Co_3O_4/$BiVO_4$ - $MoNiCuO_x$/Cu, Appl. Catal. B: Environ. 324 (2023), https://doi.org/10.1016/j.apcatb.2022.122229.

[26] C. Zhou, J. Li, Y. Zhang, J. Bai, L. Li, X. Mei, X. Guan, B. Zhou, Novel denitrification fuel cell for energy recovery of nitrate-N and TN removal based on NH_4^+ generation on a CNW@CF cathode, Environ. Sci. Technol. 56 (4) (2022) 2562–2571, https://doi.org/10.1021/acs.est.1c04363.

[27] X. Li, M. Kan, T. Wang, Z. Qin, T. Zhang, X. Qian, Y. Kuwahara, K. Mori, H. Yamashita, Y. Zhao, The ClO·generation and chlorate suppression in photoelectrochemical reactive chlorine species systems on $BiVO_4$ photoanodes, Appl. Catal. B: Environ. 296 (2021), 120387, https://doi.org/10.1016/j.apcatb.2021.120387.

[28] Y. Zhang, Y. Ji, J. Li, J. Bai, S. Chen, L. Li, J. Wang, T. Zhou, P. Jiang, X. Guan, B. Zhou, Efficient ammonia removal and toxic chlorate control by using $BiVO_4$/WO_3 heterojunction photoanode in a self-driven PEC-chlorine system, J. Hazard. Mater. 402 (2021), 123725, https://doi.org/10.1016/j.jhazmat.2020.123725.

[29] T. Li, Y. Jiang, X. An, H. Liu, C. Hu, J. Qu, Transformation of humic acid and halogenated byproduct formation in UV-chlorine processes, Water Res. 102 (2016) 421–427, https://doi.org/10.1016/j.watres.2016.06.051.

[30] T. Luo, Y. Peng, L. Chen, J. Li, F. Wu, D. Zhou, Metal-free electro-activated sulfite process for As(III) oxidation in water using graphite electrodes, Environ. Sci. Technol. 54 (16) (2020) 10261–10269, https://doi.org/10.1021/acs.est.9b07078.

[31] Y. Liu, L. Liu, Y. Wang, A critical review on removal of gaseous pollutants using sulfate radical-based advanced oxidation technologies, Environ. Sci. Technol. 55 (14) (2021) 9691–9710, https://doi.org/10.1021/acs.est.1c01531.

[32] J. Qiao, L. Feng, H. Dong, Z. Zhao, X. Guan, Overlooked role of sulfur-centered radicals during bromate reduction by sulfite, Environ. Sci. Technol. 53 (17) (2019) 10320–10328, https://doi.org/10.1021/acs.est.9b01783.

[33] L. Huang, H. Zhang, T. Zeng, J. Chen, S. Song, Synergistically enhanced heterogeneous activation of persulfate for aqueous carbamazepine degradation using Fe_3O_4@SBA-15, Sci. Total Environ. 760 (2021), 144027, https://doi.org/10.1016/j.scitotenv.2020.144027.

[34] K. Li, X. Fang, T. Wang, K. Gong, M. Ali Tahir, W. Wang, J. Han, H. Cheng, G. Xu, L. Zhang, Atmospheric organic complexation enhanced sulfate formation and iron dissolution on nano α-Fe_2O_3, Environ. Sci.: Nano 8 (3) (2021) 698–710, https://doi.org/10.1039/d0en01220c.

[35] L. Chen, M. Tang, C. Chen, M. Chen, K. Luo, J. Xu, D. Zhou, F. Wu, Efficient bacterial inactivation by transition metal catalyzed auto-oxidation of sulfite, Environ. Sci. Technol. 51 (21) (2017) 12663–12671, https://doi.org/10.1021/acs.est.7b03705.

[36] G. Wang, P. Wang, H. Liu, J. Wang, X. Dai, Y. Xin, Degradation of spiramycin by thermally activated peroxydisulfate: Kinetics study, oxidation products and acute toxicity, Chem. Eng. J. 408 (2021), 127255, https://doi.org/10.1016/j.cej.2020.127255.

[37] L. Liu, X. Xing, C. Hu, H. Wang, L. Lyu, Effect of sequential UV/free chlorine disinfection on opportunistic pathogens and microbial community structure in simulated drinking water distribution systems, Chemosphere 219 (2019) 971–980, https://doi.org/10.1016/j.chemosphere.2018.12.067.

[38] X. Wang, M. Zhu, G. Zeng, X. Liu, C. Fang, C. Li, A three-dimensional Cu nanobelt cathode for highly efficient electrocatalytic nitrate reduction, Nanoscale 12 (17) (2020) 9385–9391, https://doi.org/10.1039/c9nr10743f.

[39] C. Zhou, J. Bai, Y. Zhang, J. Li, Z. Li, P. Jiang, F. Fang, M. Zhou, X. Mei, B. Zhou, Novel 3D Pd-Cu$(OH)_2$/CF cathode for rapid reduction of nitrate-N and simultaneous total nitrogen removal from wastewater, J. Hazard. Materals 401 (2020), 123232, https://doi.org/10.1016/j.jhazmat.2020.123232.

[40] Y. Chen, G. Zhang, H. Liu, J. Qu, Confining free radicals in close vicinity to contaminants enables ultrafast fenton-like processes in the interspacing of MoS2 membranes, Angew. Chem. Int. edtion. Engl. 58 (24) (2019) 8134–8138, https://doi.org/10.1002/anie.201903531.

[41] Y. Tian, M. Zhou, Y. Pan, X. Du, Q. Wang, MoS_2 as highly efficient co-catalyst enhancing the performance of Fe^0 based electro-Fenton process in degradation of sulfamethazine: approach and mechanism, Chem. Eng. J. 403 (2021), 126361, https://doi.org/10.1016/j.cej.2020.126361.

[42] M. Zhou, S. Chen, J. Bai, J. Wang, Y. Zhang, T. Zhou, J. Li, W. Shangguan, B. Zhou, Effect of oxygen concentration and distribution on holes transfer and photoelectrocatalytic properties in hematite, Int. J. Hydrog. Energy 46 (10) (2021) 7309–7319, https://doi.org/10.1016/j.ijhydene.2020.11.245.

[43] J. Xie, J. Zhang, S. Li, F. Grote, X. Zhang, H. Zhang, R. Wang, Y. Lei, B. Pan, Y. Xie, Controllable disorder engineering in oxygen-incorporated MoS_2 ultrathin nanosheets for efficient hydrogen evolution, J. Am. Chem. Soc. 135 (47) (2013) 17881–17888, https://doi.org/10.1021/ja408329q.

[44] L. Yu, H. Zhou, J. Sun, F. Qin, F. Yu, J. Bao, Y. Yu, S. Chen, Z. Ren, Cu nanowires shelled with NiFe layered double hydroxide nanosheets as bifunctional electrocatalysts for overall water splitting, Energy Environ. Sci. 10 (8) (2017) 1820–1827, https://doi.org/10.1039/c7ee01571b.

[45] J. Lu, Y. Zhou, Y. Zhou, Efficiently activate peroxymonosulfate by Fe_3O_4@MoS_2 for rapid degradation of sulfonamides, Chem. Eng. J. 422 (2021), 130126, https://doi.org/10.1016/j.cej.2021.130126.

[46] J. Lu, Y. Zhou, J. Lei, Z. Ao, Y. Zhou, Fe_3O_4/graphene aerogels: a stable and efficient persulfate activator for the rapid degradation of malachite green, Chemosphere 251 (2020), 126402, https://doi.org/10.1016/j.chemosphere.2020.126402.

[47] H.-Q. Liu, C.-B. Yao, G.-Q. Jiang, Y. Cai, Synthesis, structure and ultrafast nonlinear absorption properties of ZnO-time/MoS_2 films, J. Alloy. Compd. 847 (2020), 156524, https://doi.org/10.1016/j.jallcom.2020.156524.

[48] Y. Qu, X. Song, X. Chen, X. Fan, G. Zhang, Tuning charge transfer process of MoS_2 photoanode for enhanced photoelectrochemical conversion of ammonia in water into gaseous nitrogen, Chem. Eng. J. 382 (2020), 123048, https://doi.org/10.1016/j.cej.2019.123048.

[49] L. Chen, X. Peng, J. Liu, J. Li, F. Wu, Decolorization of orange II in aqueous solution by an Fe(II)/sulfite system: replacement of persulfate, Ind. Eng. Chem. Res. 51 (42) (2012) 13632–13638, https://doi.org/10.1021/ie3020389.
[50] L. Zha, J. Bai, C. Zhou, Y. Zhang, J. Li, P. Wang, B. Zhang, B. Zhou, Treatment of hazardous organic amine wastewater and simultaneous electricity generation using photocatalytic fuel cell based on TiO_2/WO_3 photoanode and Cu nanowires cathode, Chemosphere 289 (2022), 133119, https://doi.org/10.1016/j.chemosphere.2021.133119.
[51] Y. Zhang, J. Li, J. Bai, X. Li, Z. Shen, L. Xia, S. Chen, Q. Xu, B. Zhou, Total organic carbon and total nitrogen removal and simultaneous electricity generation for nitrogen-containing wastewater based on the catalytic reactions of hydroxyl and chlorine radicals, Appl. Catal. B: Environ. 238 (2018) 168–176, https://doi.org/10.1016/j.apcatb.2018.07.036.
[52] R. Wang, H. Liu, K. Zhang, G. Zhang, H. Lan, J. Qu, Ni^{II}/Ni^{III} redox couple endows Ni foam-supported Ni_2P with excellent capability for direct ammonia oxidation, Chem. Eng. J. 404 (2021), 126795, https://doi.org/10.1016/j.cej.2020.126795.
[53] H. Wang, W. Guo, B. Liu, Q. Wu, H. Luo, Q. Zhao, Q. Si, F. Sseguya, N. Ren, Edge-nitrogenated biochar for efficient peroxydisulfate activation: an electron transfer mechanism, Water Res. 160 (2019) 405–414, https://doi.org/10.1016/j.watres.2019.05.059.
[54] J.A. O'Brien, J.T. Hinkley, S.W. Donne, S.E. Lindquist, The electrochemical oxidation of aqueous sulfur dioxide: A critical review of work with respect to the hybrid sulfur cycle, Electrochim. Acta 55 (3) (2010) 573–591, https://doi.org/10.1016/j.electacta.2009.09.067.
[55] E. Curcio, X. Ji, A.M. Quazi, S. Barghi, G. Di Profio, E. Fontananova, T. Macleod, E. Drioli, Hybrid nanofiltration–membrane crystallization system for the treatment of sulfate wastes, J. Membr. Sci. 360 (1–2) (2010) 493–498, https://doi.org/10.1016/j.memsci.2010.05.053.